Unstable recurrent patterns in Kuramoto-Sivashinsky dynamics

Yueheng Lan*
Department of Mechanical and Environmental Engineering, University of California, Santa Barbara, California 93106, USA

Predrag Cvitanović†
Center for Nonlinear Science, School of Physics, Georgia Institute of Technology, Atlanta, Georgia 30332-0430, USA
(Received 26 April 2008; published 18 August 2008)

We undertake an exploration of recurrent patterns in the antisymmetric subspace of the one-dimensional Kuramoto-Sivashinsky system. For a small but already rather "turbulent" system, the long-time dynamics takes place on a low-dimensional invariant manifold. A set of equilibria offers a coarse geometrical partition of this manifold. The Newton descent method enables us to determine numerically a large number of unstable spatiotemporally periodic solutions. The attracting set appears surprisingly thin—its backbone consists of several Smale horseshoe repellers, well approximated by intrinsic local one-dimensional return maps, each with an approximate symbolic dynamics. The dynamics appears decomposable into chaotic dynamics within such local repellers, interspersed by rapid jumps between them.

DOI: 10.1103/PhysRevE.78.026208 PACS number(s): 05.45.−a, 89.75.Fb, 02.60.Lj, 82.40.Ck

INTRODUCTION

Statistical approaches to the study of turbulence [1] rely on assumptions that break down in the presence of large-scale coherent structures typical of fluid motions [2]. Description of such coherent structures requires a detailed understanding of the dynamics of underlying equations of motion. In Hopf's dynamical systems vision [3], turbulence explores a repertoire of distinguishable patterns; as we watch a turbulent system evolve, every so often we catch a glimpse of a familiar whorl. At any instant and a given finite spatial resolution the system approximately tracks for a finite time a pattern belonging to a finite alphabet of admissible patterns, and the dynamics can be thought of as a walk through the space of such patterns, just as chaotic dynamics with a low-dimensional attractor can be thought of as a succession of nearly periodic (but unstable) motions.

Exploration of Hopf's program close to the onset of spatiotemporal chaos was initiated in Ref. [4], which was the first to extend the periodic orbit theory to a partial differential equation (PDE), the one-spatial-dimension Kuramoto-Sivashinsky [5,6] system, a flow embedded in an infinite-dimensional state space. Many recurrent patterns were determined numerically and the recurrent-pattern theory predictions tested for several parameter values. Continuous symmetries of the full periodic domain problem led to new important features of dynamics—such as relative periodic orbits—that merit study on their own [7]. For that reason, both in Ref. [4] and in this paper, we found it advantageous to focus on the dynamics confined to the antisymmetric subspace, the space for which periodic orbits characterize "turbulent" dynamics. In what follows we shall often refer to such periodic orbit solutions of the truncated Kuramoto-Sivashinsky equation as "recurrent patterns" in order to emphasize their spatiotemporal periodicity. In this paper (and, in much greater detail, in Ref. [8]), we venture into a Kuramoto-Sivashinsky system bigger than the one studied in Ref. [4], just large enough to exhibit turbulent dynamics arising through competition of several unstable coherent structures.

Basic properties of the Kuramoto-Sivashinsky equation are reviewed in Sec. I. The determination of equilibria and periodic orbits in high-dimensional state spaces opens new challenges, and in Sec. II we sketch the Newton descent method that we have developed and deployed in our searches for recurrent patterns. Informed by the topology of the flow, the method can determine even very long periodic orbits, such as the orbit of Fig. 6(c). Equilibria, which play a key role in organizing the global topology of state space dynamics, are investigated in Sec. III. We then fix the size of the Kuramoto-Sivashinsky system in order to illustrate our methodology on a concrete example. Not all equilibria influence the dynamics equally, and in Sec. III A we show how to gauge the relative importance of an equilibrium by its proximity to the most recurrent state space regions. For this small Kuramoto-Sivashinsky system the dynamics is shaped by the competition between "center" and "side" equilibria. In Sec. IV A we turn this observation into a dynamical description of the flow by constructing local, equilibrium-centered Poincaré sections. In Sec. IV B we show that with intrinsic curvilinear coordinates built along unstable manifolds of equilibria and short periodic orbits (the key observation of Ref. [4]), the dynamics can be reduced to iteration of low-dimensional Poincaré return maps. The long road from an infinite-dimensional PDE to essentially one-dimensional iteration is now completed, its crowning achievement the bimodal return map of Fig. 8(e). Such return maps enable us to construct a symbolic dynamics, and initiate a systematic search for periodic orbits that build up local Smale horseshoe repellers, as many as desired. The periodic points so determined are overlaid over the return map in Fig. 8(f). Interestingly, this systematic parsing of state space leads to a discovery of a nontrivial attracting periodic orbit of short period, an orbit highly unlikely to show up in random initial condition simulations of Kuramoto-Sivashinsky dynamics. The hierar-

*ylan2@engineering.ucsb.edu
†Predrag.Cvitanovic@physics.gatech.edu

chy of periodic orbits so determined can then be used to predict long-time dynamical averages via periodic orbit theory. Our results are summarized the last section.

I. KURAMOTO-SIVASHINSKY EQUATION

The Kuramoto-Sivashinsky system [2,5,6]

$$u_t = (u^2)_x - u_{xx} - \nu u_{xxxx} \tag{1}$$

arises as an amplitude equation for interfacial instabilities in a variety of physical contexts [6,9,10]. We shall study $u(x,t)$ on a periodic domain $x \in [0,L]$, $u(x,t)=u(x+L,t)$. In the Fourier space,

$$u(x,t) = i \sum_{k=-\infty}^{+\infty} a_k(t) e^{ikqx}, \quad q = 2\pi/L, \tag{2}$$

the Kuramoto-Sivashinsky PDE is represented by an infinite ladder of coupled ordinary differenential equations (ODEs) for complex Fourier coefficients,

$$\dot{a}_k = (kq)^2[1 - \nu(kq)^2]a_k - kq \sum_{m=-\infty}^{+\infty} a_m a_{k-m}. \tag{3}$$

In this paper we restrict our investigation to the subspace of odd solutions $u(x,t)=-u(-x,t)$ for which the a_k's are real. The a_0 mode is conserved since $\dot{a}_0=0$ and $a_0=\int dx\, u=0$ since u has odd parity. The linear term controls the stability of the $u(x,t)=0$ equilibrium, with each Fourier mode a_k an eigenvector of the linearized equation, with eigenvalue $\omega(kq) = (kq)^2[1-\nu(kq)^2]$. If all eigenvalues are nonpositive, the equilibrium $u(x,t)=0$ is globally stable. In general, the longest wavelengths are unstable, while the higher k contract rapidly, restricting the dynamics to a finite-dimensional inertial manifold [11,12]. The peak of the $\omega(kq)$ stability curve identifies the maximally unstable mode at $kq \approx 1/\sqrt{2\nu}$ and sets the typical wavelength of the large-system-size spatiotemporal patterns of the Kuramoto-Sivashinsky equation.

Rescaling $t \to \nu t$, $a_k \to \nu^{-1/2} a_k$, $L = 2\pi\nu^{1/2}\tilde{L}$ results in

$$\dot{a}_k = (k/\tilde{L})^2[1 - (k/\tilde{L})^2]a_k - (k/\tilde{L}) \sum_{m=-\infty}^{+\infty} a_m a_{k-m}, \tag{4}$$

where we trade in the "hyperviscosity" ν and the system size L for a single dimensionless length parameter

$$\tilde{L} = L/(2\pi\sqrt{\nu}), \tag{5}$$

which plays the role of a "Reynolds number" for the Kuramoto-Sivashinsky system. In the literature sometimes L is used as the control parameter, with ν fixed to 1, and at other times ν is varied with L fixed. In what follows we find it most convenient to set $\nu=1$ and compare different calculations in terms of either $\tilde{L}$ or L.

For small $\tilde{L}$, the dynamics and bifurcation sequences are investigated in Refs. [2,13–16]. For $\tilde{L}<1$ the equilibrium $u=0$ is the global attractor. As the system size $\tilde{L}$ is increased, the "flame front" becomes increasingly unstable and turbulent. While for $\tilde{L}$ sufficiently large the existence of many coexisting attractors is an open possibility [17], in numerical studies most initial conditions settle down in the same region of state space, the attractor with the largest basin of attraction. This is illustrated by Fig. 1 for system size $L=38.5$, $\tilde{L}=6.12\ldots$, which we shall focus on in this paper.

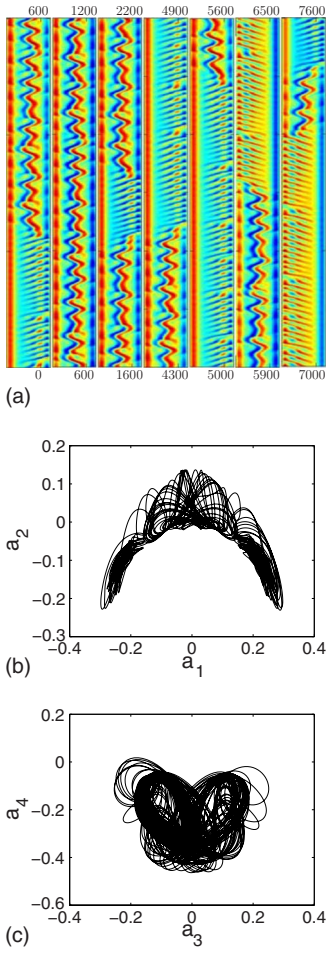

FIG. 1. (Color online) Long-time evolution of a typical "sustained turbulence" trajectory for $L=38.5$. (a) Space-time representation of $u(x,t)$ in the (x,t) plane, $x \in [0,L/2]$ horizontally, $t \in [0,7600]$, in vertical segments. The color (gray scale) represents the magnitude of $u(x,t)$. (b) (a_1,a_2) Fourier mode projection, (c) (a_3,a_4) projection. The typical time scale is set by the shortest periods of the unstable periodic orbits embedded in the central, "wobbly" and side, "traveling wave" patterns of order $T=20-25$ (see Fig. 5), so this is a very long simulation, over 300 "turnover" times. The goal of this paper is to describe the characteristic unstable wobble and traveling wave patterns in terms of a hierarchy of invariant periodic orbit solutions.

In the antisymmetric subspace the translational invariance of the full system reduces to invariance under discrete translation by $x \to x+L/2$. In the Fourier representation (4), the corresponding solution is obtained by reflection

$$a_{2m} \to a_{2m}, \quad a_{2m+1} \to -a_{2m+1}. \tag{6}$$

II. METHOD OF NEWTON DESCENT

We will investigate the properties of the Kuramoto-Sivashinsky equation in a weakly turbulent (or chaotic) regime from the perspective of periodic orbit theory [18], and refer to the application of this theory to PDEs as the *recurrent-pattern program* since here the coordination of spatial degrees of freedom plays a major role.

Christiansen *et al.* [4] proposed in 1997 that the periodic orbit theory be applied to spatiotemporally chaotic systems, using the Kuramoto-Sivashinsky system as a laboratory for exploring viability of the program. They examined its dynamics with periodic boundary condition, antisymmetric subspace, for system size $\tilde{L} \approx 5.8$, close to the onset of chaos, where a truncation of expansion (4) to 16 Fourier modes already yields accurate results. The main result was that the high-dimensional (16–64 dimensions) dynamics of this dissipative flow could be reduced to an approximately one-dimensinonal (1D) Poincaré return map, by constructing an invariant unstable-manifold-based curvilinear coordinate passing close to all unstable periodic orbits embedded within the strange attractor. A binary symbolic dynamics arising from this surprisingly simple return map made possible a systematic determination of *all* nearby unstable periodic orbits up to a given number of Poincaré section returns.

The essential limitations on the numerical studies undertaken in Ref. [4] were computational constraints: in truncation of high modes in the expansion (4), sufficiently many have to be retained to ensure that the dynamics is accurately represented; on the other hand, recurrent patterns have to be located in this high-dimensional state space. High-wave-number modes have large negative coefficients in the linear term of (4), making the system stiff and the integration slow. Basic difficulties also exist in the application of commonly used cycle-searching techniques [8,18], due to the intricate orbit structure induced by strong nonlinearity. The integration of the associated Jacobian matrix can also be expensive due to the high dimensionality.

The "Newton descent" method for determining unstable spatiotemporally periodic solutions of extended systems has been formulated and explored numerically in Refs. [19,20]. The idea of the method is to make a rough but informed guess of what the desired pattern looks like globally, and then use a variational method to drive the initial guess toward the exact solution, by minimizing a cost function computed from the deviation of the approximate flow from the true flow [Fig. 2(a)].

We initiate our searches by a long-time numerical run of the dynamics, in order to identify the frequently visited regions of the state space (natural measure), and then search for close recurrences [21]. An initial loop guess $L(0)$ is crafted by taking a nearly recurring segment of the orbit, smoothed and made periodic by a fast Fourier transform (FFT) into the wave number representation, dropping the high-frequency components, and making a FFT back to the state space. In a loop discretization each point has to be specified in all d dimensions. A typical initial loop guess is displayed in Figs. 2(b) and 2(c), along with the periodic orbit found by the Newton descent method in Fig. 2(d).

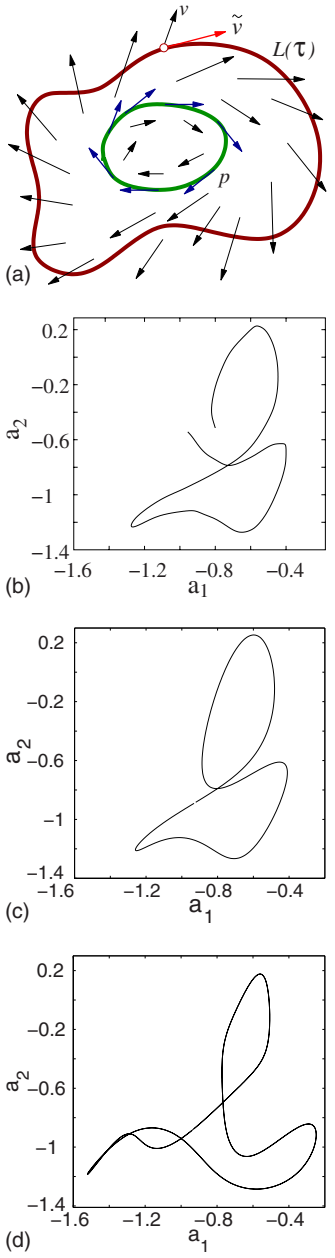

FIG. 2. (Color online) (a) The orientation of a tangent $\tilde{v}(\tilde{x})$ of the guess loop $L(\tau)$ does not coincide with the orientation of the velocity field $v(\tilde{x})$; for a periodic orbit p it does so at every $x \in p$. The Newton descent method aligns the closed loop tangent to the given vector field by driving the loop to a periodic orbit. Newton descent at work for a Kuramoto-Sivashinsky system: (b) a near return extracted from a long-time orbit, (c) initial guess loop crafted from it, and (d) the periodic orbit p reached by the Newton descent. $N=512$ points representation of the loop, (a_1, a_2) Fourier mode projection.

III. EQUILIBRIA OF THE KURAMOTO-SIVASHINSKY EQUATION

Equilibria (or steady solutions) are the simplest invariant objects in the state space. Some of them are dynamically important as they, together with their unstable or stable manifolds, partition the state space into qualitatively different re-

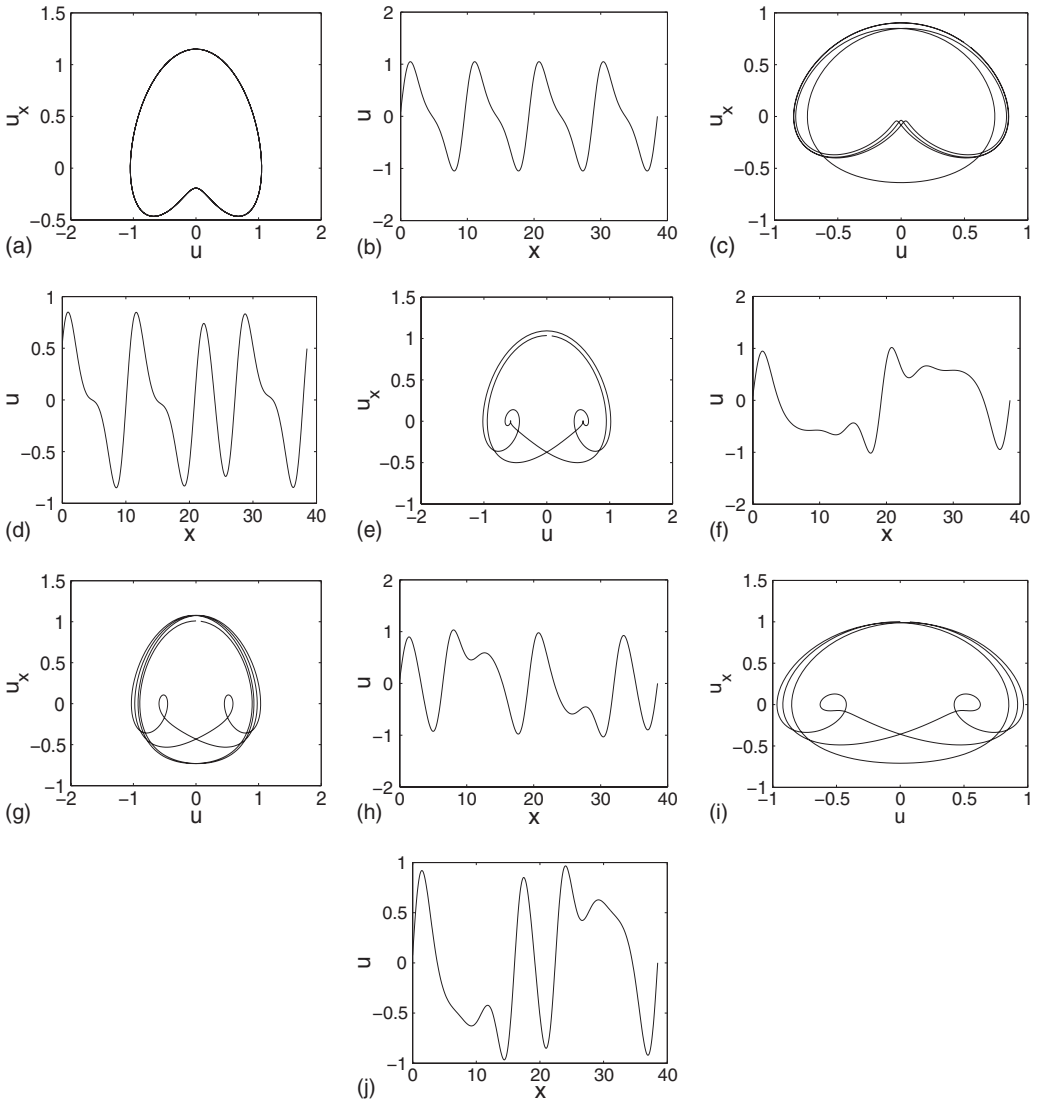

FIG. 3. Equilibria in Michelson (u,u_x) representation [23], and as $u(x)$ spatially periodic profiles: (a),(b) C_1; (c),(d) C_2; (e),(f) R_1; (g),(h) R_2; (i),(j) T. $L=38.5$, antisymmetric subspace.

gions and offer a first, coarse description of typical state space recurrent coherent structures. As we shall show here, each such region owns its own local Smale horseshoe hierarchy of unstable periodic orbits, and there are orbits communicating between different regions.

The equilibria of the Kuramoto-Sivashinsky equation (KSE) (1) satisfy

$$(u^2)_x - u_{xx} - u_{xxxx} = 0.$$

Integrating once, we get

$$u^2 - u_x - u_{xxx} = E, \tag{7}$$

where E is an integration constant [22]. Written as a 3D ODE, with spatial coordinate x playing the role of "time," this is a dynamical system [23],

$$u_x = v, \quad v_x = w, \quad w_x = u^2 - v - E, \tag{8}$$

with the "time reversal" symmetry

$$x \to -x, \quad u \to -u, \quad v \to v, \quad w \to -w.$$

Rewriting (8) as

$$(u+w)_x = u^2 - E,$$

we see that, for $E<0$, $u+w$ increases without bound as $x \to \infty$, and every solution escapes to infinity. If $E=0$, the origin (0,0,0) is the only bounded solution, a marginally stable center with eigenvalues $(0,i,-i)$.

For $E>0$ there is rich E-dependent dynamics, with fractal sets of bounded solutions. The solutions of (8) are themselves in turn organized by its own equilibria and the connections between them [23]. For $E>0$ the equilibrium points of (8) are $c_+=(\sqrt{E},0,0)$ and $c_-=(-\sqrt{E},0,0)$. Linearization of the flow around c_+ shows that c_+ has a 1D unstable manifold and a 2D stable manifold along which solutions spiral in. By the $x \to -x$ time reversal symmetry, the invariant manifolds of c_- have reversed stability properties. Most orbits escape quickly even if initiated close to the nonwandering set, and

that renders the numerical calculations difficult [24–27]. The Newton descent method [19,20] that we employ appears more robust and effective than the earlier approaches.

For a fixed spatial size L with periodic boundary conditions, the only equilibria are those with spatial periodicity L. In Fourier representation an equilibrium satisfies the infinite set of algebraic equations $\dot{a}_k=0$. In numerical computations these are truncated to a finite set of polynomial equations. In analogy with Hamiltonian dynamics, we can say that we are looking for solutions of (1) of a given spatial period L, on any E shell, rather than looking for solutions of the arbitrary period for a fixed E shell.

In the antisymmetric subspace considered here, the invariance (6) under discrete translation by $x \to x+L/2$ implies that every equilibrium solution is either invariant under a half-cell shift, or has a half-cell translated partner.

A. Search for dynamically important equilibria

For small system sizes L the number of equilibria is small and concentrated on the low-wave-number end of the Fourier spectrum. In a high-dimensional state space not all equilibria influence dynamics significantly, so we need to classify them according to their importance in shaping the long-time dynamics of (1). We gauge the relative importance of an equilibrium by its proximity to the most recurrent state space regions. Empirically, an equilibrium plays at least two roles. The larger the sum of the positive real parts of its stability exponents, and/or the more unstable eigendirections it has (for example, the $u=0$ solution), the more unlikely it is that an orbit will recur in its neighborhood: thus a highly unstable equilibrium can help elucidate the topology of an asymptotic attracting set by the "hole" that it cuts in the natural measure. On the other hand, the asymptotic dynamics can spend a large fraction of time in neighborhoods of a few "least unstable" equilibria, equilibria with only a few unstable eigendirections. Unstable manifolds of a set of such equilibria tile state space with a set of regions explored by the asymptotic dynamics.

TABLE I. Dynamically important equilibria in the antisymmetric subspace, periodic boundary conditions: value of the integration constant E, as defined in (7), and the first few least unstable stability exponents.

	E	$\mu_1 \pm i\nu_1$	$\mu_2 \pm i\nu_2$	$\mu_3 \pm i\nu_3$
C_1	0.43646	0.044	−0.255	−0.347
		$\pm i$0.261	$\pm i$0.431	$\pm i$0.463
C_2	0.25784	0.33053	0.097	−0.101
			$\pm i$0.243	$\pm i$0.233
R_1	0.36602	0.011	−0.215	−0.358
		$\pm i$0.796	$\pm i$0.549	$\pm i$0.262
R_2	0.34442	0.33223	−0.001	−0.281
			$\pm i$0.703	$\pm i$0.399
T	0.40194	0.25480	−0.07	−0.264
			$\pm i$0.645	

We pick any point on a typical orbit of (4). It corresponds to a loop in the 3D state space of (8) and so can be used to initialize the search for a $u(x)$ profile periodic in $[0,L]$. For $L=38.5$, $\nu=1$ we found in this way several dozen equilibria of (4).

Next we reinitialize the search by taking the average of an orbit segment of (4), with the hope that the typical orbit will pass through the neighborhood of important equilibria often. In this way, the number of dynamically important equilibria is greatly reduced: we find ten solutions, five of which belong to the antisymmetric subspace (see Fig. 3). The corresponding E values and leading linear stability eigenvalues are listed in Table I. No other equilibria seem to be dynamically important for this system size.

Three dynamically different regions of state space are demarcated in Fig. 1(b) by $a_1 \approx \pm 0.15$. In Table I C refers to the center in Fig. 1(b) and R to the right. The left equilibria L are omitted, as they are symmetry partners of R. The C_1

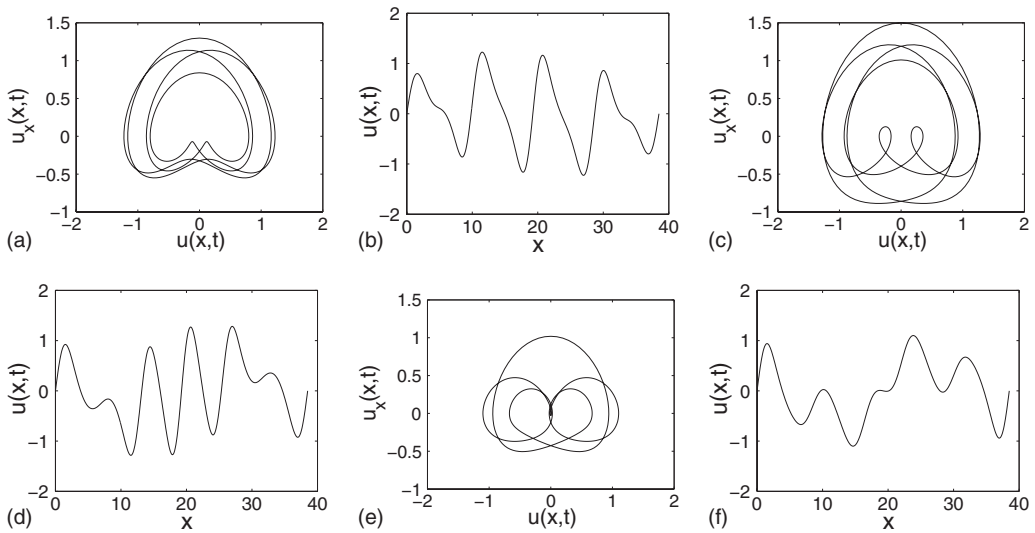

FIG. 4. Spatial profile of $u(x,t)$ at an instant t when a typical trajectory passes (a),(b) S_C, (c),(d) or S_R, (e),(f) or equilibrium T, the transition region between the central S_C and side regions S_R. Compare with Fig. 3.

equilibrium is self-dual with respect to the reflection (6), and the rest come in pairs.

The topology of equilibria is organized relative to the stationary points c_+, c_- near the unstable spiral-in manifold of c_+ and the stable spiral-out manifold of c_-. In Figs. 3(a) and 3(c), the equilibrium profiles circle the pair c_+, c_- as a whole, and u has four peaks on $[0,L]$ [see Figs. 3(b) and 3(d)]. In Figs. 3(e), 3(g), and 3(i), the profiles encircle both equilibria as well as each separately. The circulation around the two equilibria ("of equilibria") may be used to classify the solutions. Each circulation gives a peak in the u profile in $[0,L]$, with big circulations corresponding to large oscillations and small ones to the secondary oscillations.

B. Equilibria and the dynamics

Empirically, the nonwandering set appears to consist of three regions: the left part (S_L), the center part (S_C), and the right part (S_R). By the inversion symmetry (6), S_L and S_R are mirror images of each other, so only one of them needs to be considered, say S_R. Within each region the dynamics takes place on a chaotic repeller, with an orbit occasionally escaping a region and landing in the next region. Such rapid transitions show up as "defects" in the spatiotemporal evolution in Fig. 1(a).

Judged by recurrences in the long-time dynamics, the weakly unstable C_1 and R_1 appear to be the most important equilibria, with typical return times $T_i=2\pi/\nu_i$ of $T_{C_1}=24.0$ and $T_{R_1}=7.89$. In contrast, the dynamics appears to steer clear of C_2, equilibrium unstable in three eigendirections. The T equilibrium appears to mediate transitions between the side and the center regions. After checking all projections of a typical long orbit onto all (a_i,a_j) planes, we found that the dynamics frequents only the neighborhoods of the equilibria listed in Table I.

Segments of a typical orbit in the nonwandering set bear close resemblance to the equilibria listed in Fig. 3. The (u,u_x) representations and the spatial profiles of three typical instants in the long-time evolution of Fig. 4 resemble the equilibria shown in Fig. 3: Fig. 4(c) is similar to Fig. 3(c) and Fig. 4(a) is similar to Fig. 3(a). The state in Fig. 4(e), which lies along the transition from S_R to S_C, has no clear equilibrium counterpart. So, at this stage, equilibria partition the state space at the coarsest level into the alphabet $\{S_L,S_C,S_R\}$.

IV. RECURRENT PATTERNS

In this section we investigate the recurrent patterns in the KSE dynamics by constructing the unstable manifolds of dynamically important invariant sets. We define intrinsic curvilinear coordinates along unstable manifolds and then deduce return maps and construct approximate symbolic dynamics, which greatly facilitates the search for unstable periodic orbits. This program is quite successful for the "center" S_C part, but less so for the "side" S_R part.

All numerical work presented here is for system size $L=38.5$, $\nu=1$, chosen large enough to exhibit spatially nontrivial competition between various chaotic patterns. We find

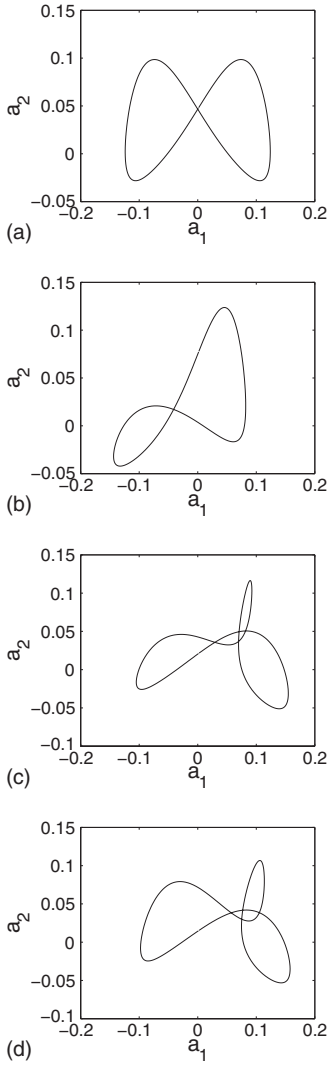

FIG. 5. (a_1,a_2) Fourier mode projection of several shortest periodic orbits in S_C. The periods are $T=$ (a) 25.6095; (b) 25.6356; (c) 36.7235; (d) 37.4083.

that the 16-Fourier-mode truncation is sufficient for our purposes [2,16]; the equilibria and periodic orbits change by a few percent if the number of modes is doubled. The translational invariance of (1) in the full state space implies that relative equilibria and periodic orbits could play important roles [28]. The restriction to the antisymmetric subspace excludes this type of solution.

A. Poincaré sections

We initialize our periodic orbit searches by checking for the nearly recurrent orbit segments. Motivated by Fig. 1(b), we choose the hyperplane $a_1=0$ as our Poincaré section for searches within S_C. The shortest unstable periodic orbits residing in S_C are displayed in Fig. 5. Each of them has a partner related by the reflection symmetry (6), except for the symmetric one, Fig. 5(a), which is self-dual under the reflection. The Poincaré section for S_R is chosen as $a_4=-0.122$. The shortest unstable periodic orbits residing in S_R are depicted in Figs. 6(a) and 6(b). Each of them has a symmetry

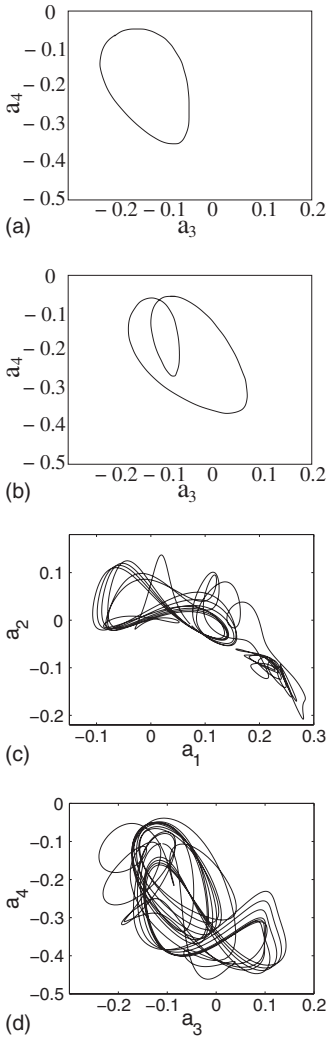

FIG. 6. (a) Shortest periodic orbit p_{R2} in S_R, $T=12.0798$, (a_3,a_4) Fourier mode projection. (b) Second shortest periodic orbit p_{R1} in S_R, $T=20.0228$, (a_3,a_4) projection. (c) (a_1,a_2) projection and (d) (a_3,a_4) projection of a long periodic orbit connecting S_C and S_R, $T=355.34$.

partner in S_L. The one in Fig. 6(a) is seen to mediate the transition from S_R to S_C, and the one in Fig. 6(b) will be used to build a symbolic dynamics in S_R. All periodic orbits that we have found have only one unstable eigendirection, enabling us to construct a 1D map to model the state space dynamics on some chosen Poincaré section.

Figures 6(c) and 6(d) show a long, period $T=355.34$, periodic orbit that communicates between S_C and S_R. We initialize the search for this orbit by choosing a segment of long-time orbit that communicates between S_C and S_R. Several of such long communicating periodic orbits are found with similar or longer periods.

The unstable manifolds of all periodic orbits found so far rarely have more than two unstable eigendirections. This is consistent with the estimated linear growth of the Hausdorff dimension of the nonwandering set with the system size [29]. In general, there exist many unstable periodic orbits with many unstable directions, but they do not appear to participate in the asymptotic dynamics. Although more than 50

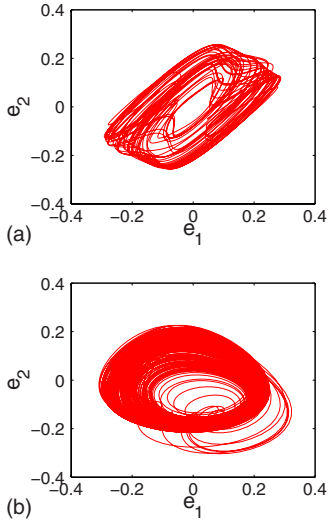

FIG. 7. (Color online) Projection of a typical state space trajectory segment onto the linearized stability eigenplanes of equilibria C_1 and R_1. The projection of part of (a) the center orbit to the eigenplane (e_1,e_2) of C_1, and (b) the right-sided orbit to the eigenplane (e_1,e_2) of R_1.

unstable periodic orbits were found in our preliminary search, we have no criterion that would preclude the possibility of more important ones yet to be detected.

In the preliminary search, we chose the Poincaré section by examining Fig. 1. A good Poincaré section is essential to the success of all subsequent steps. It should cut all the orbits in the nonwandering set transversely and should be numerically convenient; all our Poincaré sections are hyperplanes. After a Poincaré section is chosen, we determine the symbolic dynamics by examining the return map defined on the Poincaré section. In our case, the unstable manifold of the shortest orbit is nearly one dimensional and the dynamics can be approximated by maps defined on 1D line segments.

According to Table I, the least unstable equilibria C_1 and R_1 have 2D spiral-out unstable manifolds. In the neighborhood of C_1 and R_1 the unstable manifolds are well approximated by the corresponding eigenplanes determined by their complex eigenvalue pairs. The projections to the eigenplanes of nearby long-time orbit segments in Fig. 1(b) are displayed in Fig. 7. Figure 7(a) shows a projection onto the eigenplane e_1-e_2 of the center equilibrium C_1 (origin in the figure), where e_1 is the real part of the eigenvector and e_2 is then taken normal to e_1; the orbit is circling and avoiding C_1. At the left and the right bounds, there are extra orbit rotations which have a rotation plane roughly perpendicular to the e_1-e_2 eigenplane. It turns out that this rotation is related to the transition equilibrium T. Thus, the dynamics of the central part is controlled by C_1 and T (and T^*, the symmetric image of T) with the orbit spending most of the time around C_1. An obvious choice of the Poincaré section is $\mathcal{P}_C$: $\hat{a}_1=0$, where $\hat{a}_1=[\mathbf{a}-\mathbf{a}(C_1)]\cdot\mathbf{e}_1$ is the projection of the state space point $\mathbf{a}$ relative to the equilibrium C_1 along the e_1 direction. Figure 7(b) shows the projection onto the eigenplane e_1-e_2 of the right-side equilibrium R_1 [at the origin (0,0) in the figure]. We see that most of the time the orbit circles around R_1. There are many small oscillations near the bottom, in this

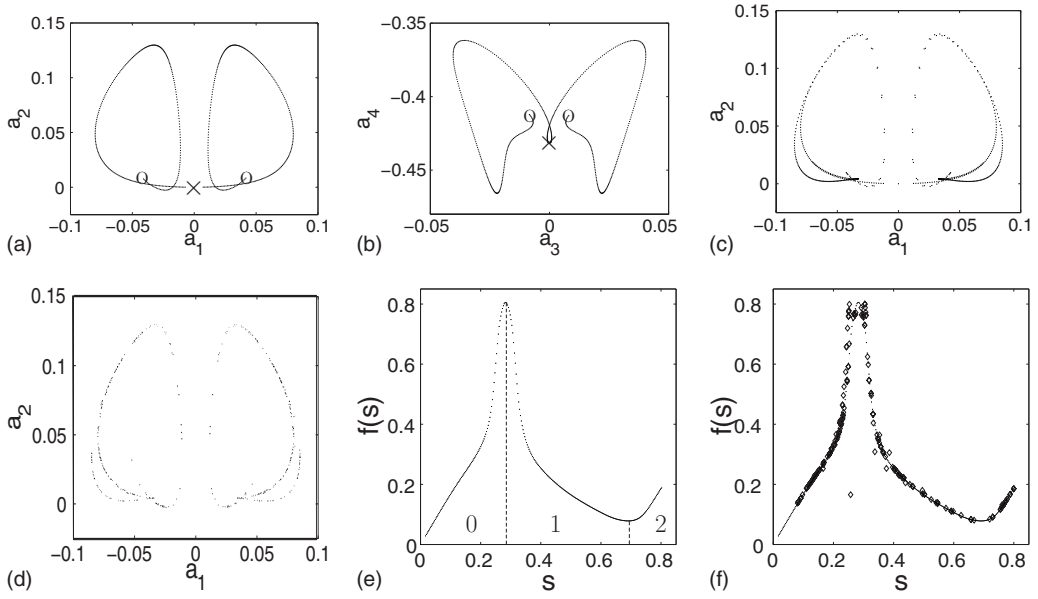

FIG. 8. (a)–(d) Fourier mode projection of the unstable manifold segment L_C of C_1 on the Poincaré section $\mathcal{P}_C$. (a) (a_1, a_2) projection of the unstable manifold on $\mathcal{P}_C$. (b) (a_3, a_4) projection (L_C is represented by 564 points). (c) Projection of the first iteration of L_C. (d) Projection of all computed unstable periodic orbits of the full domain topological length up to $n=8$. (e),(f) Poincaré return map on $\mathcal{P}_C$, the intrinsic coordinate. (e) Bimodal return map in the fundamental domain, with the symbolic dynamics given by three symbols {0, 1, 2}. × marks the position of C_1 and ○ mark the turn-back points. (f) Periodic points in the fundamental domain, overlaid over the return map (e).

projection partially masked by the dense band. In the following, $\mathcal{P}_R$: $\hat{a}_1=0$ (different from the center one) is taken to be the Poincaré section. This is not a perfect choice as the occasional tangent passage of the orbit to $\mathcal{P}_R$ can cause trouble.

B. Curvilinear coordinates, center repeller

By construction, the section $\mathcal{P}_C$ contains C_1 and the eigenvector e_2 and is perpendicular to the e_1-e_2 expanding eigenplane of C_1. We compute the intersection of the Poincaré section $\mathcal{P}_C$ with the two-dimensional unstable manifold of C_1 by iterating [30] a set of initial points on the $\pm e_2$ eigenvector, infinitesimally close to C_1. At nearest turn-back points the unstable manifold bends back sharply and then nearly retraces itself [see Figs. 8(a) and 8(b)]. Denote by L_C the "base segment" of the unstable manifold between the two nearest turn-back points that bracket C_1. Turn-back points are points on the unstable manifold for which the local unstable manifold curvature diverges for forward iterates of the map, i.e., points at which the manifold folds back onto itself arbitrarily sharply [31–33]. For our purpose, approximate turn backs suffice. Figure 8(c) shows the first iterate of L_C: finer structures do develop, but on the whole they lie close to L_C and should be well described by the intrinsic curvilinear coordinate that we now define [4].

Assign to each d-dimensional point $\hat{\mathbf{a}} \in L_C$ a coordinate $s=s(\hat{\mathbf{a}})$ whose value is the Euclidean arclength to C_1 measured along the one-dimensional $\mathcal{P}_C$ section of the C_1 unstable manifold. Next, for a nearby point $\hat{\mathbf{a}}_0 \notin L_C$ determine the point $\hat{\mathbf{a}}_1 \in L_C$ which minimizes the Euclidean distance $(\hat{\mathbf{a}}_0-\hat{\mathbf{a}}_1)^2$, and assign arclength coordinate value $s_0=s(\hat{\mathbf{a}}_1)$ to $\hat{\mathbf{a}}_0$. In this way, an approximate one-dimensional intrinsic coordinate system is built along the unstable manifold. This parametrization is useful if the nonwandering set is sufficiently thin that its perpendicular extent can be neglected, with every point on the nonwandering set assigned the nearest point on the base segment L_C.

Armed with this intrinsic curvilinear coordinate parametrization, we are now in a position to construct a one-dimensional model of the dynamics on the nonwandering set. If $\hat{\mathbf{a}}_n$ is the nth Poincaré section of a trajectory in the neighborhood of C_1, and s_n is the corresponding curvilinear coordinate, then $s_{n+1}=f(s_n)$ models the full state space dynamics $\hat{\mathbf{a}}_n \to \hat{\mathbf{a}}_{n+1}$. We define $f(s_n)$ as a smooth, continuous one-dimensional map f: $L_C \to L_C$ by taking $\hat{\mathbf{a}}_n \in L_C$, and assigning to $\hat{\mathbf{a}}_{n+1}$ the nearest base segment point $s_{n+1}=s(\hat{\mathbf{a}}_{n+1})$.

This Poincaré return map is multimodal and, due to the discrete symmetry (6), antisymmetric under the $s \to -s$ reflection. This discrete symmetry (6) can be profitably used to simplify the symbolic dynamics [18]. Defining the $s \geqslant 0$ segment as the fundamental domain, the return map for the fundamental domain is partitioned by two points {0.2825, 0.6905} into a three-letter alphabet {0,1,2} [see Fig. 8(e)]. The chaos generating mechanism—stretching and folding—is clearly illustrated by this return map. The dynamics can now be approximated by a subshift of finite type in the space of symbol sequences built from these three letters [18,34].

The distribution of the points on the return map is highly nonuniform. This is consistent with the Poincaré section Fig. 8(c) for which the vertical segments in the middle contain fewer representative points than other segments. Our studies indicate that the dynamics in this region of state space is controlled by the "transition" equilibrium T. T has a much stronger repulsion rate ($\mu_T \sim 0.2548$) than the C_1 equilibrium ($\mu_{C_1} \sim 0.044\,22$; see Table I). A line segment is strongly stretched by a close passage to T, and its representative

TABLE II. Cycles up to topological length 4 for the center repeller in the fundamental domain; cycles up to topological length 8 for the side repeller. Listed are the topological lengths, the itineraries p, the largest Lyapunov exponents $\lambda_p = \ln|\Lambda_{p,1}|/T_p$, periods T_p, and the first three (four) stability eigenvalues (to save space, complex eigenvalue pairs are labeled by a single index). Our approximate symbolic dynamics fails to resolve cycles 0001 and 0001*.

	p	λ_p	T_p	Λ_1	Λ_3	Λ_4
			Center periodic orbits			
1	1	0.0946	12.8047	−3.3581	0.20299	0.008861
2	01	0.07363	25.6356	−6.6028	0.004697	−0.0003854
3	001	0.05814	38.7241	−9.5000	0.0001186	3.687817783×10^{-5}
	011	0.0698	38.4520	14.6402	5.0398×10^{-5}	0.00029158
	002	0.04558	37.8160	8.6967	1.01538×10^{-4}	5.1672×10^{-5}
4	0001	0.04647	52.5998	−11.5219	1.3912×10^{-5}	-3.4661×10^{-7}
	0001*	0.05511	57.7721	−24.1326	4.1012×10^{-5}	-6.6332×10^{-5}
	0011	0.05736	51.8915	19.6194	-7.5089×10^{-5}	$2.3526\pm i2.4938\times10^{-8}$
	0111	0.07977	51.2393	−59.5683	0.0001284	-1.0469×10^{-8}
	0002	0.047	57.3329	14.802	7.8781×10^{-6}	-5.0674×10^{-7}
	0012	0.05103	58.0857	−19.3765	-6.9811×10^{-5}	-3.5525×10^{-8}
			Side periodic orbits			
1	0	0.02747	20.0228	−1.7333	−0.433	$0.001158\pm i0.0002633$
2	01	−0.006163	40.0565	$-0.5569\pm i0.5479$	1.4892×10^{-6}	1.2363×10^{-6}
6	000001	0.01113	120.1658	−3.8073	−0.05628	-4.03×10^{-10}
7	0000101	0.02363	140.196	−27.4733	−0.006032	-6×10^{-12}
8	00001001	0.03375	160.2561	223.2796	0.0005662	-1.202×10^{-9}

points get very sparse upon one Poincaré iteration. This indicates that the dynamics in the center region of state space is coarsely organized by the two equilibria C_1 and T.

The return map $f(s)$ leads to approximate finite Markov diagrams and the associated symbolic dynamics, enabling us to search for unstable periodic orbits in a systematic fashion. Up to length 4, the pruning rule implied by Fig. 8(e) precludes symbol sequences {21,22,202,2010}. We find all unstable periodic orbits of period n within S_C by first determining the zeros of the one-dimensional map $f^n(s)$ [i.e., the n-periodic points of $f(s)$], and then initiating the Newton descent by the corresponding points in the full state space. Whenever the 1D model map is a good representation of the full state space dynamics, this approach yields a periodic orbit for every admissible itinerary, of arbitrary period.

For the center region S_C the return map of Figs. 8(e) and 8(f) appears to be a good description of the full state space dynamics. We found all admissible orbits up to length 8, and list the orbits of fundamental domain periods up to 4 in Table II. The cycles with n odd are symmetric under the reflection (6), while the cycles with n even are either self-dual or have a symmetry partner. A few examples are plotted in Fig. 9.

All unstable periodic orbits we found in S_C have one unstable eigendirection, with other eigendirections highly contracting, which partially justifies the 1D description of the dynamics. Figure 8(d) shows the $\mathcal{P}_C$ periodic points of periods up to 8; the set agrees well with the unstable manifold section of Fig. 8(c). Figure 8(f) displays the return map in the fundamental domain reconstructed from these periodic points. It matches well the map Fig. 8(e), with the exception of an "outlier" cycle, denoted 0001* in Table II, which shares the symbol sequence with cycle {0001}. The same outlier is visible in the center of the lower left quadrant of Fig. 8(d). This point lies on another branch of the attractor, defined by a different turn-back point. Cycles depicted in Figs. 5(a), 5(c), 5(d), 9(c), and 9(d) also belong to other branches, and are not listed in Table II. There are infinitely many turning points and unstable manifold folds; our description accounts for only one important part of S_C.

To summarize: the approximate one-dimensional dynamics based on the closest turn-back pair interval bracketing the C_1 equilibrium unstable manifold suffices to establish the existence of a Smale horseshoe in this neighborhood. A more accurate description would require inclusion of further turn backs [35,36].

C. Side repeller

The dynamics within the side repeller S_R appears more complicated than the one discussed above for the center S_C. In this case our local Poincaré return map captures only a small (though important) subset of the S_R nonwandering set. For the S_R case, we utilize the unstable manifold of the $n=1$ cycle shown in Fig. 6(b) and listed in Table II as cycle 0. The unstable manifold has two intersections with the Poincaré section $\mathcal{P}_R$; we take the upper one (along e_2) as the origin from which to measure arclength s. The 1D unstable eigenvector of the 0 cycle fundamental matrix is then used to construct the one-dimensional, arclength-parametrized base segment of the unstable manifold L_R, as in the preceding section and Ref. [30]. We represent it numerically by 82

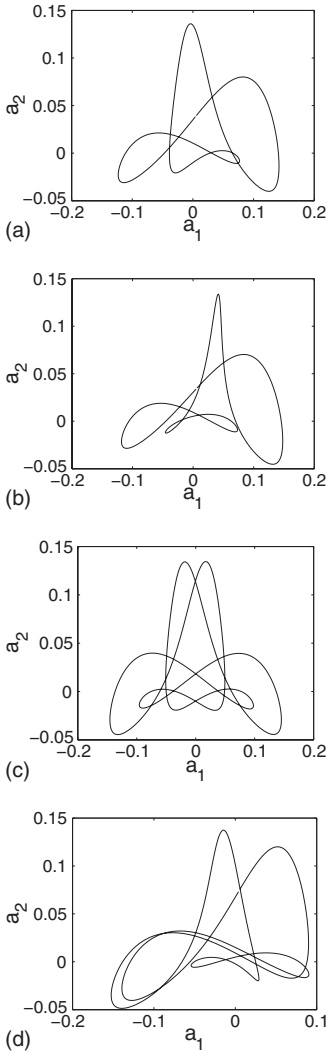

FIG. 9. (a_1,a_2) Fourier mode projection of two cycles in S_C listed in Table II: (a) cycle 0011, (b) cycle 0012. Two short typical cycles not listed in the table: (c) a symmetric unstable periodic orbit in S_C with the period $T=77.4483$, (d) an asymmetric unstable periodic orbit in S_C with the period $T=81.3345$.

points. Figures 10(a) and 10(b) show the (a_1,a_2) and $(a_3\ a_4)$ Fourier mode projections of L_R.

Figure 10(c) shows the first iterate of L_R, with a clear indication of a turn back. Figure 10(d) indicates a second turn back arising from the second iteration of L_R. Higher iterations show still finer turn-back structures. The approximate return map displayed in Fig. 10(e) is unimodal, with the two symbols {0,1} representing the two monotone laps, partitioned by the critical point at $s=0.034$. The corresponding pruning rules up to length 8 preclude the existence of sequences {11,1001,10000}, so the set of admissible subsequences up to length 8 is {0,01,0001,000101,00010101}.

The search based on this symbolic dynamics yields cycles up to length $n=8$ listed in Table II. Note that the 01 cycle is attractive, and thus not part of the repeller S_R. This approximate symbolic dynamics predicts that all cycles of lengths $n=6,7,8$ are pruned; nevertheless such cycles do exist. Furthermore, the admissible sequences such as 0001 have no corresponding unstable periodic orbits. Figure 10(f) shows the unstable manifold return map superimposed on the one constructed from the periodic points (diamonds). The return map here captures only the gross features of the overall dynamics of the unstable periodic orbits. All this indicates that in this case our simple one-dimensional model dynamics is not as good a description as that for S_C.

To summarize, the Newton descent enables us to determine all symbolic dynamics admissible unstable periodic orbits on S_C up to topological length $n=8$. The Poincaré return map guided Newton descent searches for S_R were not as successful, yielding only the small set of unstable periodic orbits listed in Table II.

However, even the partial knowledge of symbolic dynamics implied by the approximate return map of Fig. 10(e) leads to a very interesting discovery of the *attracting* periodic orbit of period $T=40.0565$, Fig. 11(a). A nearby unstable periodic orbit of period $T=60.1112$ of similar appearance is shown in Fig. 11(b). In studies of turbulence in fluids the only known stable solutions are the laminar equilibria, but, from the dynamical systems point of view, for higher-dimensional flows any number of coexisting attractors can exist. The above nontrivial stable state would never be observed in a long-

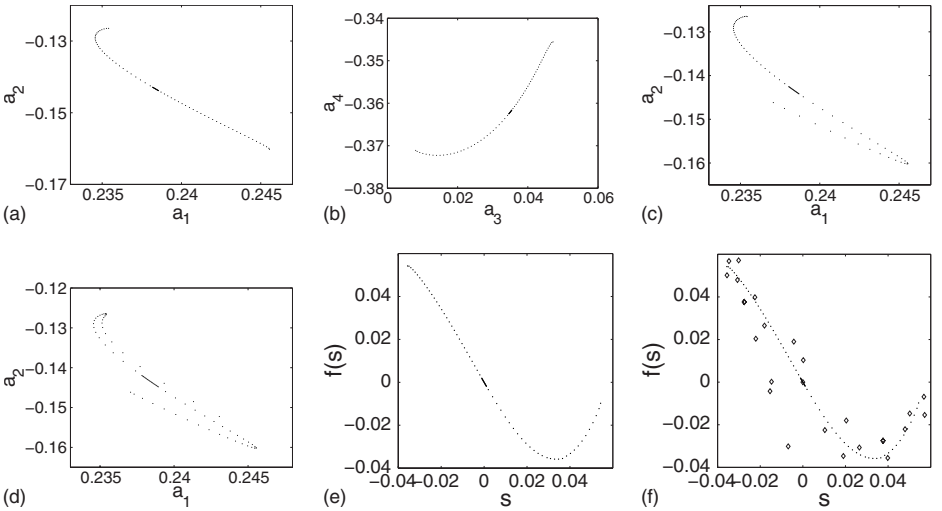

FIG. 10. Fourier mode projections of the unstable manifold L_R of 0 cycle on the Poincaré section $\mathcal{P}_R$: (a) (a_1,a_2) and (b) (a_3,a_4) projection of the unstable manifold on $\mathcal{P}_R$. Projection of (c) the first iteration of L_R and (d) the second iteration of L_R. (e),(f) The Poincaré return map on $\mathcal{P}_R$, intrinsic coordinate: (e) Unimodal return map, with alphabet {0,1}. (f) The return map reconstructed from the periodic points (diamonds). For comparison, the unstable manifold return map is indicated by the dots.

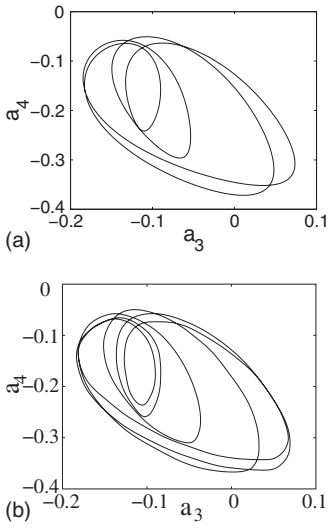

FIG. 11. (a) (a_3,a_4) Fourier mode projection of the attracting periodic orbit 01 within S_R. (b) A nearby unstable periodic orbit within S_R.

time, random initial conditions numerical simulation of the flow, as its immediate basin of attraction is an exceedingly small island embedded within the "sustained turbulence" region of state space.

SUMMARY

The recurrent-pattern program was first implemented in detail [4] on the 1D Kuramoto-Sivashinsky system at the onset of chaotic dynamics. For these specific parameter values, many recurrent patterns were determined numerically and the periodic orbit theory predictions tested. In this paper we venture into a large Kuramoto-Sivashinsky system, just large enough to exhibit turbulent dynamics of topologically richer structure, arising through competition of several unstable coherent structures. Both papers explore dynamics confined to the antisymmetric subspace, a space for which periodic orbits characterize turbulent dynamics. Reference [7] studies the Kuramoto-Sivashinsky system in the full periodic domain, where relative periodic orbits due to the continuous translational symmetry play a key role, and Ref. [37] applies the lessons learned to a full 3D Navier-Stokes flow. In this context, Kawahara and Kida [38] have demonstrated that the recurrent patterns can be determined in turbulent hydrodynamic flows by explicitly computing several important unstable spatiotemporally periodic solutions in the three-dimensional plane Couette turbulence.

We have applied here the recurrent-pattern program to the Kuramoto-Sivashinsky system in a periodic domain, antisymmetric subspace, in a larger domain size than explored previously [4]. The state space nonwandering set for a system of this particular size appears to consist of three repelling Smale horseshoes and orbits communicating between them. Each subregion is characterized by qualitatively different spatial u profiles in the 1D physical space. The recurrent patterns, identified in this investigation by nearby equilibria and periodic orbits, capture well the state space geometry and dynamics of the system. Both the equilibria and periodic orbits are efficiently determined by the Newton descent method. The equilibria so determined, together with their unstable manifolds, provide the global frame for the nonwandering set. We utilize these unstable manifolds to build 1D curvilinear coordinates along which the infinite-dimensional PDE dynamics is well approximated by one-dimensional return maps and the associated symbolic dynamics. In principle, these simple models of dynamics enable us to systematically classify and search for recurrent patterns of arbitrary periods. For the particular examples studied, the approach works well for the central repeller but not so well for the side repeller.

The above advances are a proof of principle, first steps in the direction of implementing the recurrent-pattern program. But there is a large conceptual gap to bridge between what has been achieved, and what needs to be done: Even the flame flutter has been probed only in its weakest-turbulence regime, and it is an open question to what extent Hopf's vision remains viable as such spatiotemporal systems grow larger and more turbulent.

[1] U. Frisch, *Turbulence* (Cambridge University Press, Cambridge, UK, 1996).
[2] P. Holmes, J. L. Lumley, and G. Berkooz, *Turbulence, Coherent Structures, Dynamical Systems and Symmetry* (Cambridge University Press, Cambridge, UK, 1998).
[3] E. Hopf, Comm. Pure Appl. Math. **1**, 303 (1948).
[4] F. Christiansen, P. Cvitanović, and V. Putkaradze, Nonlinearity **10**, 55 (1997).
[5] Y. Kuramoto, Suppl. Prog. Theor. Phys. **64**, 346 (1978).
[6] G. I. Sivashinsky, Acta Astronaut. **4**, 1177 (1977).
[7] P. Cvitanović, R. L. Davidchack, and E. Siminos, e-print arXiv:0709.2944.
[8] Y. Lan, Ph.D. thesis, Georgia Tech, 2004.
[9] H. C. Chang, Annu. Rev. Fluid Mech. **26**, 103 (1994).
[10] H. C. Chang, Phys. Fluids **29**, 3142 (1986).
[11] R. Temam, *Infinite-Dimensional Dynamical Systems in Mechanics and Physics* (Springer, New York, 1988).
[12] C. Foias, B. Nicolaenko, G. R. Sell, and R. Temam, J. Math. Pures Appl. **67**, 197 (1988).
[13] J. M. Hyman and B. Nicolaenko, Physica D **18**, 113 (1986).
[14] I. G. Kevrekidis, B. Nicolaenko, and J. C. Scovel, SIAM J. Appl. Math. **50**, 760 (1990).
[15] D. Armbruster, J. Guckenheimer, and P. Holmes, SIAM J. Appl. Math. **49**, 676 (1989).
[16] M. E. Johnson, M. S. Jolly, and I. G. Kevrekidis, Int. J. Bifurcation Chaos Appl. Sci. Eng. **11**, 1 (2001).
[17] J. M. Hyman, B. Nicolaenko, and S. Zaleski, Physica D **23**, 265 (1986).
[18] P. Cvitanović, R. Artuso, R. Mainieri, G. Tanner, G. Vattay, N. Whelan, and A. Wirzba, *Chaos: Classical and Quantum* (Niels

Bohr Institute, Copenhagen, 2008).
[19] P. Cvitanović and Y. Lan, in *Proceedings of 10th International Workshop on Multiparticle Production: Correlations and Fluctuations in QCD*, edited by N. Antoniou (World Scientific, Singapore, 2003).
[20] Y. Lan and P. Cvitanović, Phys. Rev. E **69**, 016217 (2004).
[21] D. Auerbach, P. Cvitanović, J.-P. Eckmann, G. Gunaratne, and I. Procaccia, Phys. Rev. Lett. **58**, 2387 (1987).
[22] J. M. Greene and J. S. Kim, Physica D **33**, 99 (1988).
[23] D. Michelson, Physica D **19**, 89 (1986).
[24] S. Bouquet, J. Math. Phys. **36**, 1242 (1995).
[25] A. P. Hooper and R. Grimshaw, Wave Motion **10**, 405 (1988).
[26] H. E. Nusse and J. A. York, Physica D **36**, 137 (1989).
[27] P. Moresco and S. P. Dawson, Physica D **126**, 38 (1999).
[28] V. López, P. Boyland, M. T. Heath, and R. D. Moser, SIAM J. Appl. Dyn. Syst. **4**, 1042 (2005).
[29] S. Tajima and H. S. Greenside, Phys. Rev. E **66**, 017205 (2002).
[30] C. Simo, in *Les Méthodes Modernes de la Mécanique Céleste (Goutelas '89)*, edited by D. Benest and C. Froeschlé (Editions Frontieres, Gif-sur-Yvette, 1989), pp. 285–329.
[31] P. Cvitanović, G. H. Gunaratne, and I. Procaccia, Phys. Rev. A **38**, 1503 (1988).
[32] A. Politi, R. Badii, and P. Grassberger, J. Phys. A **21**, 763 (1988).
[33] F. Christiansen and A. Politi, Phys. Rev. E **51**, R3811 (1995).
[34] R. Gilmore and C. Letellier, *The Symmetry of Chaos* (Oxford University Press, Oxford, 2007).
[35] K. T. Hansen, Ph.D. thesis, University of Oslo, 1993, ChaosBook.org/projects/theses.html
[36] P. Cvitanović and K. T. Hansen, Nonlinearity **11**, 1233 (1998).
[37] J. F. Gibson, J. Halcrow, and P. Cvitanović (unpublished).
[38] G. Kawahara and S. Kida, J. Fluid Mech. **449**, 291 (2001).